Energy 109 (2016) 974–986

Contents lists available at ScienceDirect

Energy

journal homepage: www.elsevier.com/locate/energy

Dynamic simulator and model predictive control of an integrated solar combined cycle plant

Carolina V. Ponce [a], Doris Sáez [b], Carlos Bordons [c], Alfredo Núñez [d, *]

[a] University of La Serena, La Serena, Chile
[b] University of Chile, Santiago, Chile
[c] University of Seville, Seville, Spain
[d] Delft University of Technology, Delft, The Netherlands

ARTICLE INFO

Article history:
Received 29 May 2015
Received in revised form
12 March 2016
Accepted 29 April 2016

Keywords:
Integrated solar combined cycle power plant
Solar-collector-based steam generator
Combined cycle power plant
Supervisory model predictive control

ABSTRACT

This paper presents the design and evaluation of a dynamic simulator for an ISCC (integrated solar combined cycle) plant. The design of the simulator is based on the phenomenological equations for both a combined cycle plant and a solar plant. The simulator incorporates a regulatory control strategy based on PI (proportional-integral) controllers and was developed in the MATLAB/Simulink® environment. A MPC (model predictive control) strategy established at a supervisory level is presented. The intent of the strategy is to regulate the steam pressure of the superheater of the ISCC plant. The combined use of the simulator and the supervisory control strategy allows for the quantification of the reduction in fuel consumption that can be achieved when integrated solar collectors are used in a combined cycle plant. The ISCC plant simulator is suitable for designing, evaluating and testing control strategies and for planning the integration of solar and combined cycle plants.

1. Introduction

The construction of ISCC (integrated solar combined cycle) power plants has provided a remarkable technological contribution toward sustainable power generation [7]. In addition, the integrated construction of such plants is highly effective because CC (combined cycle) plants can operate more efficiently than other types of plants. An ISCC power plant features three main components: a CC thermal power plant, a distributed collector field and a solar steam generator. The solar steam generator is the component that connects the solar collector plant to the combined cycle plant and allows for the transfer of energy between them. Fig. 1 shows a diagram of an ISCC plant consisting of a high-temperature gas turbine, a steam turbine and a solar collector plant. Steam for the turbine is provided by two sources: the boiler and the solar field [1]. Preheated feed water is extracted from the high-pressure preheater, evaporated and slightly superheated in the solar steam generator. Then, it goes to the boiler, and together with the steam from the conventional evaporator, it is superheated to reach the steam temperature.

The first electric power generation plant to integrate a combined cycle plant with a distributed solar collector (i.e., an ISCC plant) is located in HassiR'mel, Algeria [6]. The plant features a 150 MW combined cycle generator with a solar share of 30 MW_{el} net (or 35 MW_{el} gross). The cost to build the plant was 425 million USD. The solar plant consists of a field of distributed solar collectors; thermal oil (the heat transfer fluid, HTF) circulates through a tube at a temperature of 393 °C at the outlet of the field. The largest ISCC plant in the world is located in Ain Beni Mathar, Morocco. Egypt [13] and Iran [14] also have ISCC plants in which hot oil is used as the transfer fluid. Italy, through its Archimedes Project, operates a 750 MW plant with 5 MW of solar energy; in this plant, a molten salt eutectic mixture (60% NaNO3 and 40% KNO3) is used as HTF. Due to the high solidification temperature of the molten salts (around 290 °C), other options like the direct production of steam in the solar collector or the use of gaseous fluids like CO_2 as HTF are being studied [11]. Florida, USA, also possesses several ISCC plants, with 74 MW of solar energy. To the best of our knowledge, the most recently constructed plant of this type is Agua Prieta II in Mexico (470 MW with a solar contribution of 14 MW). Similar plants are also being constructed in Australia and India [1]. The plants located

* Corresponding author.
E-mail addresses: cponce@userena.cl (C.V. Ponce), dsaez@ing.uchile.cl (D. Sáez), bordons@us.es (C. Bordons), a.a.nunezvicencio@tudelft.nl (A. Núñez).

http://dx.doi.org/10.1016/j.energy.2016.04.129

Nomenclature

ARIX	Auto-Regressive Integrated with Exogenous input
CC	Combined Cycle
HP	High Pressure
HRSG	Heat Recovery Steam Generation
HTF	Heat Transfer Fluid
ISCC	Integrated Solar Combined Cycle
MPC	Model Predictive Control
SSG	Solar Steam Generator
$f(L)$	Function depending on drum shape
I_{wF}	Indicator of fuel used in kg/s
$\overline{IJ}$	Global index for the total objective function
$\overline{IJ}_{Cr}$	Global index for the regulatory term
$\overline{IJ}_{Cf}$	Global index for the fuel cost
J	Objective function
J_{Cr}	Objective function regulatory term
J_{Cf}	Objective function fuel-cost term
t_{sim}	Simulation time s

Nomenclature and values

C_{pa}	Specific heat of oil $J/(kg \cdot K)$, 3795.5
C_v	Specific heat of steam from the drum $J/(kg \cdot K)$, 5000
C_f	Fuel cost per flow unit US$/(kg/s), 798
C_{gm}	Specific heat of steam from the SSG $J/(kg \cdot K)$, 5000
C_{st}	Heat capacitance of the superheater tubes $J/(kg \cdot K)$, 481.4
C_{ps}	Specific heat of steam at constant pressure $J/(kg \cdot K)$, 2330
f_s	Superheater friction coefficient m^{-4}, 2615
h_s	Specific enthalpy of superheated steam J/kg, 3.3117×10^6
h_{ref}	Reference steam enthalpy J/kg, 3.32×10^6
h_v	Specific enthalpy of saturated steam (drum) J/kg, 2.7977×10^6
h_a	Attemperator water specific enthalpy J/kg, 5.5217×10^6
h_e	Feed water specific enthalpy, 5.6217×10^5
h_f	Specific enthalpy of evaporation J/kg, 1.987×10^6
h_{gm}	Specific enthalpy of SSG steam J/kg, 2.8087×10^6
h_w	Specific enthalpy of liquid water J/kg, variable
h_{wv}	Specific enthalpy of saturated water J/kg, variable
K_{ec}	Coefficient $kg/(K^*s)$, 0.6124
k_s	Experimental heat transfer coefficient $J/(kg^*K)$, 4.37×10^4
k_i	Integral constant, 2×10^{-8}
k_p	Proportional constant, 3×10^{-6}
L^*	Reference drum level m, 4.1425
M_s	Mass of the superheater tubes kg, 1.04×10^4
m_a	Oil mass flow from the storage tank of the solar plant kg/s, 3.6491
m_{d1}	Drum liquid mass kg, 3817.6
p_{eg}	SSG inlet water mass flow pressure Pa, 2.9×10^6
p_G	Furnace gas pressure Pa, 1.013×10^5
p_s	Superheated steam pressure Pa, 4.5251×10^6
p_s^r	External steam pressure set point Pa, 4.5251×10^6
p_s^*	Steam pressure set point Pa, 4.5251×10^6
$\widehat{p}_s$	Steam pressure step-ahead prediction, variable
p_v	Steam drum pressure Pa, 4.5417×10^6
p_{vgm}	SSG inlet water mass flow pressure $mm\ hg$, 21.75×10^3
P_G	Gas turbine power MW, 34
P_s	Steam turbine power MW, 11
P_G^*	Gas turbine power set point MW, 34
P_s^*	Steam turbine power set point MW, 34
Q_{gs}	Heat supplied to the superheater (from the furnace) J/s, 3.0117×10^6
Q_s	Heat transferred to the steam J/s, 5.6105×10^6
Q_a	Heat supplied to the oil from solar radiation J/s, 2.7003×10^6
Q_{gm}	Heat supplied to the SSG steam J/s, 2.7003×10^6
R_s	Ideal gas constant for water $Pa \cdot m^3/kg \cdot {}^oK$, 461.5
T_a	Inlet temperature of the oil from the storage tank of the solar plant K, 568
T_w	Water temperature in the drum K, 526.76
T_g	Outlet temperature of the superheated steam K, variable
T_{gm}	Steam temperature of the SSG K, 505.017
T_v	Saturated steam temperature in the drum K, 505
T_{st}	Superheater metal tube temperature K, 735.3078
T_s	Superheated steam temperature K, 717.72
T_t	Superheater inlet steam temperature K, 526.52
T_{ref}	Reference steam temperature K, 723.15
T_0	Saturated steam temperature at pipe pressure, K 505
v_{dow}	Volumetric liquid flow rate through downcomer m^3/s, 0.71556
V	Drum volume m^3, 9.253
V_L	Drum liquid volume m^3, 4.8425
V_s	Superheater volume m^3, 8.462
V_v	Vapor volume m^3, 4.4105
w_{gm}	Steam mass flow from the SSG kg/s, 1.2
w_{gm}^*	Reference steam mass flow from the SSG kg/s, 1.2
w_{eg}	Inlet mass flow of liquid water kg/s, 1.2
w_F	Fuel mass flow kg/s, variable
w_T	Total superheated steam mass flow kg/s, 13.2
w_v	Steam mass flow from the drum to the superheater kg/s, 12
w_e	Water flow from the economizer kg/s, 12
w_{ec}	Liquid mass evaporation from the drum, 0
w_d	Water mass flow to the downcomer kg/s, 564.11
w_r	Liquid vapor mixture mass flow kg/s, 564.11
w_s	Steam mass flow out of the superheater kg/s, 10.8
w_A	Air steam mass flow kg/s, 64.093
w_{at}	Attemperator water mass flow kg/s, 0
α, β, λ	Weighting parameters, 10^8, 1, 10^2
τ_g	Empirical time constant of flow s, 1
ρ_T	Total superheated steam density kg/m^3, 13.662
ρ_s	Superheated steam density kg/m^3, 13.662
ρ_v	Saturated steam density kg/m^3, 22.763
ρ_w	Drum water density kg/m^3, 788.34
x	Steam quality, variable
$xs1$	Dummy variable J/m^3, 4.524×10^7

in Morocco, Algeria and Egypt cost 416 million Euros, 315 million Euros and 150 million Euros, respectively, to construct. Nezammahalleh et al. [17] have reported that the levelized energy cost of the Iranian ISCC plant is 76.45 USD/MWhe. Given that the ISCC technology is relatively new, various technical and economic studies, such as those by Horn et al. [13] and Hosseini et al. [14], have been conducted to evaluate the feasibility of such plants in various geographical locations. The factors that have been evaluated include thermal efficiency and capacity, environmental considerations, investment, and fuel cost. It has been concluded that

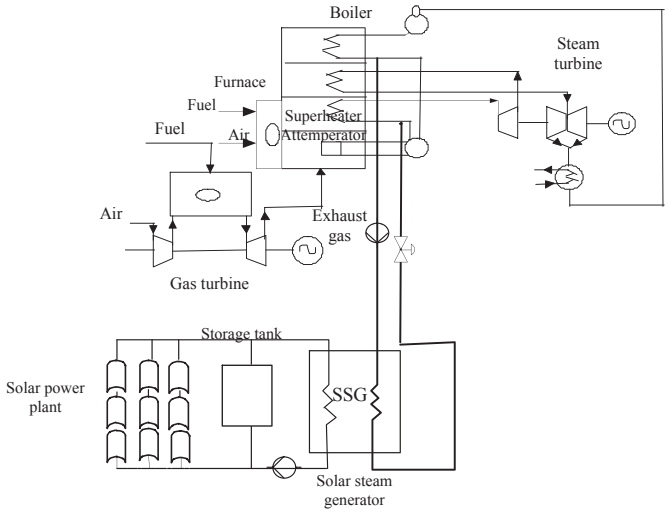

Fig. 1. ISCC diagram.

operating an ISCC plant is more commercially viable than operating a single solar power plant and that ISCC plants are capable of providing environmental and economic benefits for electric power generation. Amelio et al. [2] evaluate the performance of an innovative ISCC plant, considering linear parabolic collectors where the heat transfer fluid is the same oxidant air that is introduced into the combustion chamber. With this configuration, the net average year efficiency is 60.9% against the 51.4% of a reference combined cycle plant without solar integration.

A thermodynamic evaluation of the ISCC plant located in Yazd, Iran, was performed by Baghernejad and Yaghoubi [4,5]. The energy and exergy of the solar field and the ISCC plant were analyzed, and the thermoeconomics required to minimize the cost of investment in equipment and the cost of exergy in the ISCC plant were considered. Al-Sulaiman [3] also conducted an exergy analysis of a solar collector plant, including the analysis of an ISCC plant that produces steam via the Rankine cycle. Several refrigerants were examined, and among the combined cycles that were examined, the combined cycle known as R134a demonstrated the best exergetic performance, with a maximum exergetic efficiency of 26%. Kelly et al. [15] searched for the optimal method of transferring solar thermal energy from a combined cycle plant to produce electrical energy. Among the three investigated alternatives, the most efficient method was to remove the feed water from the heat recovery steam generator, downstream from the second-stage economizer (with the highest temperature), thereby producing high-pressure saturated steam, and then to return the steam to the heat recovery steam generator to be superheated and reheated by the gas turbine exhaust gases. Cau et al. [11] analyzed the behavior of an ISCC plant in which the heat transfer fluid is CO_2. The results indicated that the energy conversion efficiency of such plants is slightly better than that of systems based on steam cycles and is very similar to that of systems that generate electricity directly from steam. Nezammahalleh et al. [17] performed a conceptual design and technical/economic evaluation of a combined cycle plant with integrated solar collectors for the direct generation of electricity from steam. This technology was compared with the ISCC plant in Iran, in which oil is used as the HTF, and with a solar power plant. The authors concluded that the cost of the ISCC plant, which generates electricity directly from steam, is lower than that of the other two systems.

Nowadays, different ways to integrate a combined cycle-plant with solar power plants are possible. One of those ways is by using solar tower power plants as in Spelling et al. [23]. In Ref. [23], a thermo-economic optimization is performed, minimizing the investment costs and the levelized electricity costs by using an evolutionary multi-objective optimization algorithm. An efficiency around 18–24% can be reach, depending on the initial investment. Lambert et al. [16] analyze the energy cost of CO_2 capture for a natural gas combined cycle plant, and the integration with a solar tower system. Different cases are studied, including the exhaust gas recirculation and the pre-combustion case that uses the exhaust gas recirculation with the capture being realized after the compression stage of the gas turbine. It was found that addition of solar energy reduces the total energy costs.

Because of the importance ISCC plants have attained, it necessary to develop simulators that model these plants to satisfy various objectives, such as the evaluation of control strategies, optimization, or planning. Cau et al. [11] used the software GateCycle® for the evaluation of ISCC plants. GateCycle® enables the design of CC plants, fossil boiler plants, cogeneration systems, combined heat and power plants, advanced cycle gas turbines, and many other energy systems. The software can be used for evaluation, design, remodeling, re-powering, and acceptance testing. However, this software does not include models of solar collectors; therefore, the authors first developed a model for solar collector plants and then evaluated a CC plant using GateCycle®. Aftzoglou [1] performed a study of an ISCC plant from the thermodynamic perspective based on the principle of overheating. For this study, the simulator CycleTempo was used. CycleTempo is a tool for the thermodynamic analysis and optimization of systems designed for the production of electricity, heat and refrigeration. It should be noted that both the GateCycle® software and the simulator proposed by Aftzoglou [1] are steady state simulators whose purpose is the design of ISCC plants. By contrast, the simulator proposed in this paper is a dynamic simulator for the design and dimensioning of ISCC plants, the study and design of control strategies, and dynamic optimization. Thus, this paper presents a new and, to the best of our knowledge, unique contribution to ISCC plant design because no other dynamic simulator of this type has yet been reported in the literature.

2. Plant description

The ISCC power plant analyzed in this study corresponds to the integration of a CC plant with both a supplementary fired boiler and a distributed solar collector plant. The idea is to replace some fraction of the steam produced by the supplementary fired boiler with steam produced in a steam generator that uses oil heated in a solar collector plant. The integration of the solar plant into the CC plant was achieved following the study by Kelly et al. [15].

2.1. Combined cycle power plants

In a CC power plant, a gas turbine and a steam turbine are used to generate electrical power. The exhaust gas from the gas turbine is used to generate steam in the boiler. The boiler extracts heat from the exhaust gas to increase the temperature and pressure of the steam. In a CC plant with a supplementary fired boiler, in addition to the heat recovered from the exhaust gas, an additional firing is provided to the boiler, thereby increasing the amount of steam produced. The electrical efficiency may be lower than that of the standard configuration (without a supplementary firing to the

boiler), but there is additional flexibility in that the boiler may be supplied with a different type of fuel from that of the turbine [18].

2.2. Solar collector plants

The solar power plant considered in this paper is a solar thermal plant featuring parabolic collectors. The parameters considered in the simulator emulate the operation of the real plant located in the desert of Tabernas, Southern Spain. The plant consists of a field of 480 distributed solar collectors grouped into 20 rows and 10 parallel loops. Each loop has a length of 172 m, and the total open surface area is 2672 m^2. The primary objective of this type of solar plant, namely, one based on a distributed collector field, is to collect solar energy by heating oil that is passing through the field. The field is also provided with a tracking system, which causes the mirrors to revolve around an axis parallel to the pipe, thereby enabling the collectors to reduce the angle between the rays of the sun and a vector normal to the aperture of the collector (angle of incidence). Cold inlet oil is extracted from the bottom of the storage tank and passed through the field by a pump located at the field inlet. This fluid is heated and then returned to the storage tank. The type of oil used in this plant is Santotherm 55. The operating temperature range is −25 °C to 290 °C. In many parts of the world, especially Europe, Solutia markets Therminol 55 HTFs under the name of either Santotherm 55 or Gilotherm 55. This fluid has a low thermal conductivity, and its density is highly dependent on temperature. One storage tank can be used to contain both hot and cold oil. The tank used in this field has a capacity of 140 m^3, which allows for the storage of 2.3 thermal MWh; it has an inlet temperature of approximately 210 °C and an outlet temperature of approximately 290 °C [8].

3. The ISCC dynamic simulator

A dynamic simulator for a combined cycle power plant with integrated solar collectors (i.e., an ISCC plant) was developed using MATLAB/Simulink®. The design is based on a simulator for a solar collector plant, ACUREX [8], and on the combined cycle plant simulator developed by Sáez et al. [22], which is based on the phenomenological equations presented by Ordys et al. [17]. This simulator is useful for studying the behavior of variables relevant to an ISCC plant, for comparing the dynamics of an ISCC plant with those of a CC plant and for ISCC plant design. Among the relevant variables to consider are the fuel flow from the furnace, the drum level, the steam pressure in the superheater and the furnace gas pressure. The simulator is also designed to assess the reduction in the fuel consumption of the furnace relative to the fuel consumption of CC plants. The simulator was developed for a 45 MW combined cycle thermal power plant consisting of a boiler, a P_s = 11 MW steam turbine and a P_g = 34 MW gas turbine. The available simulator for the ACUREX solar plant is able to deliver a peak thermal power of 1.2 MW. Various representative examples of ISCC plants can generate higher power. In this paper, the primary objective of the scale test simulator is to reproduce the most relevant phenomenological processes of ISCC plants. For the integration of a solar plant and a SSG (solar steam generator) into a combined cycle plant, it is necessary to add certain equipment, such as pumps and valves, in addition to adapting the equations that describe the dynamics of the CC plant superheater. The equations that describe the dynamics of the drum do not change. According to Ordys et al. [18], the equations for the drum are as follows:

$$w_e + (1-x)w_r - w_d - w_{ec} = \frac{d}{dt}(m_{d1}) \tag{1}$$

$$\frac{m_{d1}}{\rho_w} = f(L) \quad L = f^{-1}\left(\frac{m_{d1}}{\rho_w}\right)$$

$$V_L = f(L) = \pi r^2 L \tag{2}$$

$$w_d = v_{dow}\rho_w \tag{3}$$

$$w_e h_e + (1-x)w_r h_{wv} = w_d h_w + w_{ec} h_v + \frac{d}{dt}(m_{d1} h_w) \tag{4}$$

$$w_{ec} + x w_r - w_v = \frac{d}{dt}(V_v \rho_v) \tag{5}$$

$$w_{ec} = K_{ec}(T_w - T_v) \tag{6}$$

$$V_v = V - V_L \tag{7}$$

where equation (1) represents the liquid mass balance, (2) the drum liquid level, (3) the downcomer mass flow, (4) the liquid heat balance, (5) the steam mass balance, (6) the evaporation dynamics and (7) the vapor volume.

In designing the dynamic simulator for an ISCC plant, the following assumptions were adopted:

- The solar plant has its own field controller that keeps the outlet oil set point temperature for changing weather conditions. This controller adjusts the oil flow in the solar field in order to reject the disturbances caused by the variation of solar radiation along the day and changes in the return inlet oil temperature. The solar plant has a storage tank which provides energy from which the oil that passes to the solar steam generator is extracted and decouples both parts of the plant. So, although the oil flow is not fixed (since it is continually manipulated by the solar field controller), the solar support can be considered constant. Therefore, when the solar field is in operation, the thermal energy supplied by the storage tank is kept at its nominal value.
- From the previous assumption, it follows that the temperature of the oil inlet to the solar steam generator can be held constant during day-to-day planning operations.
- The water mass flow from the feed water to the drum in the CC plant is the same as the water mass flow from the feed water to the drum in the ISCC plant.
- The gas turbine and the steam turbine are similar in both the CC and ISCC simulators. The only difference is the source of energy used to heat the steam.
- Basic PI controllers are considered because they are typically implemented efficiently in real plants for the control of steam pressure, drum level, furnace gas pressure, superheated steam temperature, exhaust gas temperature, NO_x concentration in exhaust gas and turbine mechanical power. Thus, the PI control loops of the ISCC plant simulator are similar to those of the CC plant simulator. A feedforward controller is incorporated for the feed water supplied to the SSG.

3.1. Design of the solar steam generator simulator

An SSG uses oil that was previously heated in a solar collector plant and then stored in an energy storage tank. The heat of the oil

is transferred to liquid water, producing steam that then passes into the combined cycle plant. The oil from the solar plant has a certain temperature T_a and a given mass flow m_a. The inlet liquid water in the SSG has an enthalpy h_w and a temperature T_w, but as it flows through the heat exchanger and the water is heated to the saturated steam temperature corresponding to the inlet flow pressure p_{eg}, saturated steam with a steam enthalpy of h_{gm} is produced. Subsequently, the output emits a steam flow that corresponds to w_{gm} and a heat flow of Q_{gm}. Fig. 2 shows a schematic diagram of the heat interchange process between the oil from the storage tank of the solar plant and the water from the HRSG (heat recovery steam generator) of the CC plant.

As described by Dersch et al. [12], Price et al. [19] and Kelly et al. [15], the SSG was designed by considering an inlet water flow of 10% of the water flow injected into the drum of the CC plant.

The characteristics of the oil from the ACUREX solar collectors were also considered, i.e., the specific heat, temperature and mass flow of the oil. Fig. 3 presents a diagram that depicts the inputs and outputs of the SSG simulator. The inlet water mass flow pressure p_{eg} is derived from the pump used to increase the water flow pressure from the feed water (Fig. 1), and saturated steam is obtained in the SSG. The equations that describe the SSG are as follows:

$$C_{pa} = 1820 + 3.478T_a \tag{8}$$

$$T_0 = \frac{3816.4}{18.304 - \ln\left(p_{vgm}\right)} + 46.13 \tag{9}$$

$$h_{gm} = -1.8934 \cdot 10^6 + 4.1404 \cdot 10^4 T_0 - 148.7585 \cdot T_0^2 + 0.2471 \cdot T_0^3 - 1.5519 \cdot 10^{-4} \cdot T_0^4 \tag{10}$$

$$Q_a = m_a C_{pa}(T_a - T_0) \tag{11}$$

$$Q_{gm} = -Q_a \tag{12}$$

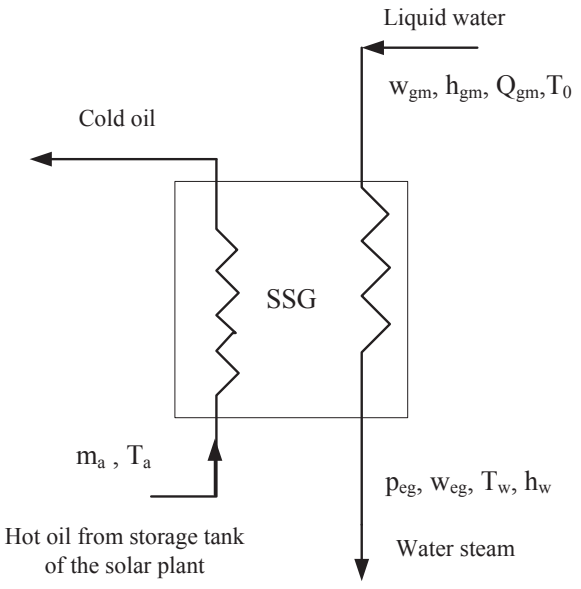

Fig. 2. Schematic diagram of the process of heat interchange from the hot oil originating from the solar plant to the steam water injected into the boiler.

$$\frac{d}{dt}w_{gm} = (w_{eg} - w_{gm})/\tau_g \tag{13}$$

where (8) to (12) are algebraic equations and (13) a differential equation. Equation (8) describes the specific heat of the oil Therminol 55 as a function of its temperature. Other properties of the oil, such as its thermal conductivity, dynamic viscosity and Prandlt number, also depend on the temperature [9], [10]. Equation (9) is the steam saturation temperature as described by Reid et al. [20]. Saturated steam is produced at a high temperature and then enters the superheater. Equation (10) represents the enthalpy of saturated steam as a function of the steam temperature, as suggested in a study conducted by Reynolds [21]. In Equation (11), the heat transferred to the oil from solar radiation is a function of the oil temperature and the steam saturation temperature. Equation (12) is a heat balance, heat received by the steam in the heat exchanger is equal to the heat provided by the oil; thus, heat losses are negligible. The steam flow at the outlet of the steam generator (w_{gm}) can be obtained using equation (13), where the speed of the steam flow equals the difference between the inflow to and outflow from the exchanger divided by a time constant (τ_g).

In the SSG simulation process, the values of T_a and m_a from the solar plant are read. w_{eg} and p_{eg} are also read, where the first variable is derived from the feed water and the second is obtained from the pump installed at the outlet of the feed water. The initial SSG conditions and parameters are defined. Algebraic equations (8)–(12) are solved. Then, w_{gm} is obtained via equation (13) using w_{eg} and τ_g. The values obtained for h_{gm}, Q_{gm}, T_o and w_{gm} are applied to the superheater. This loop is repeated at each sampling time step. The attemperator is part of the superheater. The inflow to the superheater is w_T, whereas w_s corresponds to the outflow of the superheater, which is the steam at the input to the turbine. Both are shown in Fig. 3.

In Fig. 3 the control loop in the drum regulates its level by opening or closing the valve when the level is lower or higher than the reference. The control loop in the steam turbine keeps the turbine power near the power reference demand by changing the flow of steam coming from the superheater. If power demand increases, the valve is opened to increase the mass flow of superheated steam. If the power demand decreases, the valve is closed to reduce the steam flow. The water supply of the steam generator also has a control loop and it works similarly to the control level of the drum. The reference value in this case corresponds to the amount of liquid water that could be converted into steam in the SSG (Solar Steam Generator).

3.2. Design of the ISCC simulator

As previously stated, the design of the ISCC simulator considered in this study is based on the CC simulator developed by Sáez et al. [22] with the integration of a solar plant [8]. The same equipment is considered in the design of both the CC and solar plants, with the only difference being the energy source that heats a fraction of the steam going to the superheater. In general, the models were developed using the basic principles of conservation of energy, mass and momentum. The SSG output steam, w_{gm}, is injected into the boiler of the combined cycle plant in the superheater stage. The injected steam is added to the steam from the drum w_v. All steam present in the superheater, w_T, is heated to a superheated state. Finally, the superheated steam, w_s, is injected into the steam turbine in the HP section (high-pressure). The equations that describe the dynamics of the superheater are as follows:

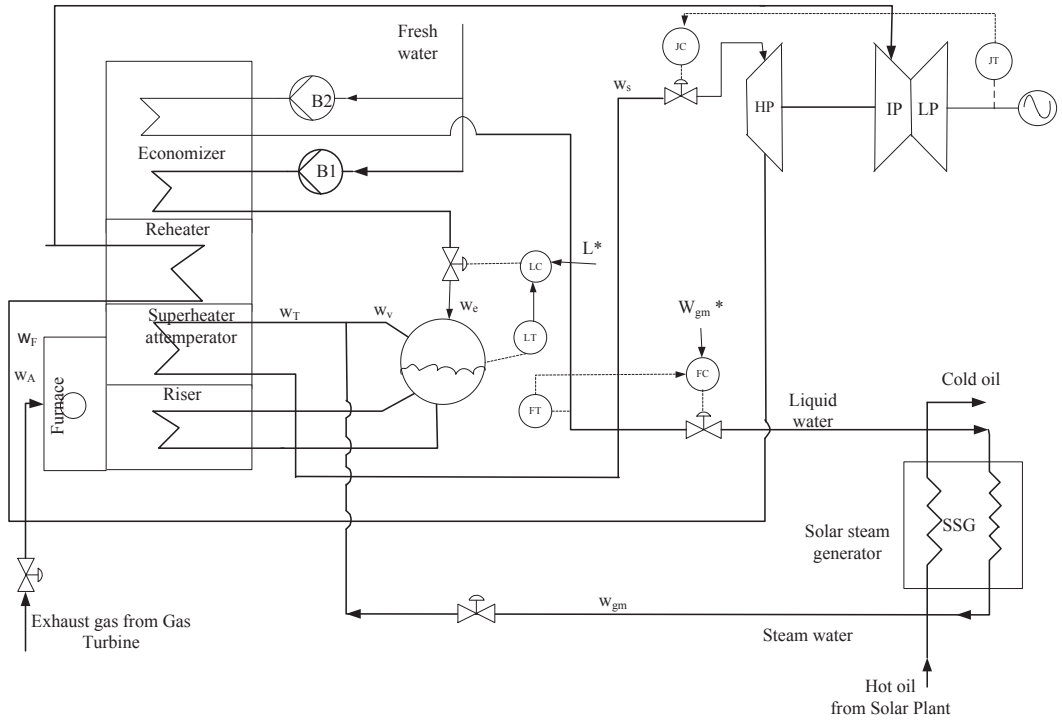

Fig. 3. SSG connected to a CC plant.

$$p_v - p_s = \frac{w_T^2}{\rho_T} f_s \tag{14}$$

$$Q_s = k_s w_T^{0.8}(T_{st} - T_s) \tag{15}$$

$$\begin{aligned} \Delta h &= C_{ps}\left(T_s - T_{ref}\right) \\ T_s &= \left(h_s - h_{ref}\right)\Big/ C_{ps} + T_{ref} \end{aligned} \tag{16}$$

$$p_s = R_s \rho_s T_s \tag{17}$$

$$w_v C_v (T_t - T_v) = w_{gm} C_{gm} \left(T_{gm} - T_t\right) \tag{18}$$

$$T_t = \frac{w_v T_v + w_{gm} T_{gm}}{w_v + w_{gm}} \tag{19}$$

$$w_v - w_s + w_{gm} + w_{at} = V_s \frac{d}{dt}(\rho_s) \tag{20}$$

$$Q_{gs} + Q_{gm} = Q_s + M_s C_{st} \frac{d}{dt}(T_{st}) \tag{21}$$

$$Q_s + w_v h_v + w_{gm} h_{gm} = w_s h_s - \left(h_a - h_f\right) \cdot w_{at} + V_s \frac{d}{dt}(\rho_s h_s) \tag{22}$$

where (14) to (19) are algebraic equations, and (20) to (22) are differential equations. The losses due to friction that are generated in the pipelines where the total steam (w_T) passes to the steam turbine are estimated based on momentum balance in equation (14). Equation (15) was empirically deduced and describes the heat transfer between the metal (pipelines) and the steam, considering turbulent flow. As in equation (14), the total steam is considered in the relation. The superheated steam temperature is obtained using equation (16), where the variation in the enthalpy between a temperature T_s and the reference temperature T_{ref} is calculated under the assumption of ideal conditions. Assuming an ideal gas model, where R_s is the universal gas constant, the superheated steam pressure is obtained in equation (17). The total steam generated in the superheater originates from two sources, the SSG and the exhaust gas turbine. The temperatures of these two sources are different. A mixture of both flows must be considered in the energy balance, as in equation (18). Under the assumption of a constant heat capacity $C_v \approx C_{gm}$, the temperature of the inlet steam that arrives at the superheater is obtain using equation (19). Through mass balance, the total steam in the superheater is obtained in equation (20). The inflow is equal to the outflow of the superheater; thus, losses are negligible. Note that in (20), an average behavior of density along the pipe is considered. This assumption could be relaxed and in a future work the steam density changes along the pipe could be modeled. In equation (21) is the superheater heat balance. The heat that is transferred to the steam, according to the furnace model, incurs losses in the pipelines through which the steam flows (final term of the equation). The heat balance equation (22) for steam includes the energy provided by the steam from the SSG; therefore, this balance equation is different from that presented by Sáez et al. [22].

In the first step of the superheater simulation process, w_a, w_s, p_v, Q_{gs}, h_v, h_o, w_{gm}, h_{gm}, Q_{gm}, T_{gm}, and T_o are measured. The superheater parameters are defined, and the initial conditions for *xs1*, h_s and p_s are provided. Then, *xs1* is calculated. Algebraic equations (14)–(19) are solved. Then, differential equations (20)–(22) are solved. P_s, T_s, h_s, and ρ_s are sent to the steam turbine. The loop is repeated at each sampling time. Other routines used in the simulator have already been implemented and reported by Ordys et al. [18] and Sáez et al. [22]. At the beginning of the paper, the nomenclature and the variable ranges used in the simulators are specified.

4. Model predictive control at the supervisory level for an ISCC plant

A MPC (Model Predictive Control) strategy at the supervisory level for ISCC plants was designed. The output of the supervisory level scheme is used as a set point for the steam pressure in the boiler at the regulatory level. Fig. 4 illustrates a scheme for such a control strategy. The external set point p_s^* is constant and corresponds to the steady-state superheater steam pressure.

The output variables of the boiler are the furnace pressure of the gases (p_G), the temperature of the steam at the outlet of the boiler (T_S) and the level of the drum of the CC plant (L). These variables are controlled using PI (proportional-integral) controllers at the regulatory level. For the supervisory control strategy, the input is p_s and the output is p_s^r.

4.1. System identification

For the supervisory-level model, an ARIX (Auto-Regressive Integrated with Exogenous input) model was established for the outlet pressure of the steam flow of the superheater, p_s, as a function of the fuel flow of the afterburner, w_F. For the design of the supervisory-level control scheme, a data set was obtained from the simulator by varying the reference pressure (p_s^r) and adding pseudorandom binary noise. The reference values were varied between 3.5×10^6 and 5.4×10^6 Pa. Furthermore, a model for the regulatory-level PI controllers was obtained for the fuel flow w_F as a function of p_s^r. The sampling time of this model is $t_m = 10$ s, and its structure is as follows:

$$A\left(z^{-1}\right)p_s(t) = B\left(z^{-1}\right)w_F(t) + \frac{e(t)}{\Delta} \tag{23}$$

where $e(t)$ is white noise; z^{-1} is the delay operator, $z^{-1}y(t) = y(t-1)$; $\Delta = 1 - z^{-1}$; and the polynomials $A(z^{-1})$ and $B(z^{-1})$ are of 13th order:

$$\begin{aligned} A\left(z^{-1}\right) = {} & 1 + a_1 z^{-1} + a_2 z^{-2} + a_3 z^{-3} + a_4 z^{-4} + a_5 z^{-5} + a_6 z^{-6} \\ & + a_7 z^{-7} + a_8 z^{-8} + a_9 z^{-9} + a_{10} z^{-10} + a_{11} z^{-11} \\ & + a_{12} z^{-12} + a_{13} z^{-13} \end{aligned}$$

$$\begin{aligned} B\left(z^{-1}\right) = {} & b_1 z^{-1} + b_2 z^{-2} + b_3 z^{-3} + b_4 z^{-4} + b_5 z^{-5} + b_6 z^{-6} \\ & + b_7 z^{-7} + b_8 z^{-8} + b_9 z^{-9} + b_{10} z^{-10} + b_{11} z^{-11} \\ & + b_{12} z^{-12} + b_{13} z^{-13} \end{aligned}$$

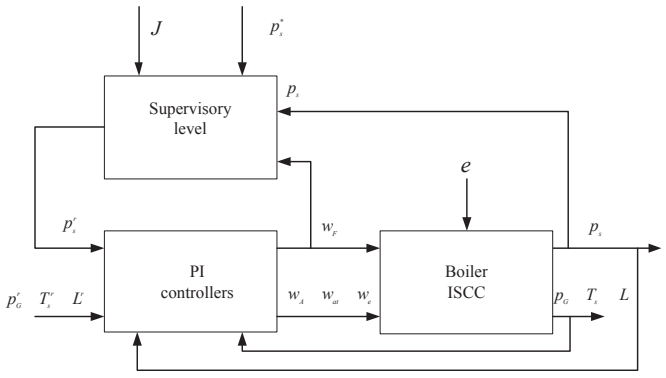

Fig. 4. Control scheme including supervisory level.

This model was obtained by evaluating the RMS (Root Mean Square) errors between the actual values and the values obtained using ARIX models of different orders (structure optimization). The model with the lowest RMS error was thus selected. To calculate the control variable w_F, a PI controller is considered as follows:

$$w_F(s) = \left(K_p + \frac{K_i}{s}\right)\left(p_s^r(s) - p_s(s)\right) \tag{24}$$

where $K_p = 3 \times 10^{-6}$, $K_i = 2 \times 10^{-8}$, $p_s^r(s)$ is the reference pressure for the superheated steam, and $p_s(s)$ is the real pressure of the superheated steam.

4.2. Objective function

The objective function used for the supervisory MPC strategy is given by

$$J = J_{Cr} + \lambda J_{Cf} \tag{25}$$

$$J_{Cr} = \alpha \sum_{k=1}^{N} \left(\widehat{p}_s(t+k) - p_S^*\right)^2 + \beta \sum_{k=1}^{N} \Delta w_F^2(t+k-1) \tag{26}$$

$$J_{Cf} = \sum_{k=1}^{N} C_f w_F(t+k-1) \tag{27}$$

and the following operational constraints over the fuel flow are included:

$$10 \le w_F(t+k-1) \le 14.5, \quad k = 1, \ldots, N \tag{28}$$

Where $\widehat{p}_s(t+k)$ is the k-step-ahead prediction for the reference pressure, $w_F(t+k-1)$ is the fuel flow and $\Delta w_F(t+k-1)$ is the control effort at instant $t+k-1$. The first term in equation (25) is a regulatory term, whereas the second term optimizes the fuel costs. In equation (26), the second term accounts for the optimization of the control effort together with the tracking error. In equation (27), C_f is the fuel cost per flow unit in US$/(kg/s). The minimum and maximum values defined in constraint equation (28) are chosen from Ref. [18] and they correspond to the constraints over the start-up and the maximum admissible fuel flow of the CC plant. Finally, the decision variable p_s^r is obtained by minimizing the objective function of equation (25), considering the corresponding constraints and using the PI controller model given by equation (28).

4.3. Parameter tuning of the supervisory MPC strategy

In equations (25) and (26), the weights (λ, α, β) are obtained from the design of the objective function. Each of these weights represents the relative importance of the function by which it is multiplied. To optimize these variables, we adopted a simulation-based approach in which, for a fixed value of $\beta = 1$, different values of α and λ were tested over the entire simulation period. A broad range of values were evaluated. Based on global performance statistics, the optimal tuning parameters were obtained; in this case, these parameters were found to be $\alpha = 10^8$ and $\lambda = 10^2$. To consider the performance of the system over the entire simulation period t_{sim}, each pair of parameters was assessed based on global statistics:

$$\overline{IJ} = \frac{1}{t_{sim}} \sum_{k=1}^{t_{sim}} J(k) = \frac{1}{t_{sim}} \sum_{k=1}^{t_{sim}} \left(J_{Cr}(k) + \lambda J_{Cf}(k)\right) \tag{29}$$

$$\overline{IJ}_{Cr} = \frac{1}{t_{sim}} \sum_{k=1}^{t_{sim}} J_{Cr}(k) \tag{30}$$

$$\overline{IJ}_{Cf} = \frac{1}{t_{sim}} \sum_{k=1}^{t_{sim}} J_{Cf}(k) \tag{31}$$

where equation (29) is the global performance index for the total objective function, equation (30) is the global performance index for the regulatory term, and equation (31) is the global index for the fuel cost. Using these parameters, good overall controller performance was achieved, with a reasonable trade-off between the tracking error on the pressure of the steam in the boiler and the reference value given by the supervisory MPC scheme, while maintaining minimal burning of the fuel at the auxiliary burner.

4.4. Performance index

To compare the fuel consumption between a CC plant and an ISCC plant, the amount of fuel saved is defined as the amount of fuel consumed by the CC plant minus the amount of fuel consumed by the ISCC plant; under the assumption that the amount of fuel used by the CC plant corresponds to 100%, the percent reduction in the amount of fuel supplied to the furnace is calculated as the amount of fuel consumed by the CC plant minus the amount of fuel consumed by the ISCC plant, divided the amount of fuel consumed by the CC and multiplied by 100. To compare the performance of the ISCC plant with and without the implementation of the supervisory MPC strategy, the following global indicator of the fuel used at the auxiliary burner was defined:

$$I_{wF} = \frac{1}{t_{sim}} \sum_{k=1}^{t_{sim}} w_F(k) \tag{32}$$

5. Simulation results

5.1. Comparison of the ISCC plant with the CC plant

To validate the behavior of the ISCC plant simulator, several simulations were performed, as many with the ISCC simulator as with the CC simulator. The results obtained for different cases and using different variables were compared. The behaviors of both the controlled and manipulated variables of the boiler were studied. The controlled variables that were studied included the steam pressure in the superheater, p_s; the drum level, L; the pressure of the gases in the furnace, p_G; and the temperature of the superheated steam in the superheater, T_s. The manipulated variables that were studied included the flow of fuel from the auxiliary burner of the furnace, w_F; the water flow from the economizer, w_e; the air flow from the auxiliary burner of the furnace, w_A; and the mass flow of water from the attemperator, w_{at}. Manipulated variables are also known as decision variables. The purpose was to optimize those variables such that the ISCC plant exhibited both good tracking performance and reduced fuel costs. Two cases are presented: one in which a supervisory controller was used, and one in which a PI controller was used. To illustrate the behavior of the controllers, a step-function change in the reference value of the steam pressure was applied, and the dynamic response is presented in Fig. 5. After 40 s approx., the transient responses are observed for both controllers achieving the new set-point. The overshoot is lower with the supervisory controller compared with the PI control strategy.

A downward step of 10% was applied to the set point of the gas turbine power (P_G^*) and to the set point of the steam turbine power (P_s^*). This downward step was applied in three different cases: first for the CC plant simulator, then for the ISCC plant simulator with 10% steam support from the SSG and, finally, for the ISCC plant simulator with 20% solar support. The objective of these simulations was to vary the behavior of the controlled and manipulated variables pertaining to the furnace before the addition of steam support from the SSG and, in particular, to verify that the flow of fuel, w_F, diminishes when solar plant support is added. Fig. 6 shows the results obtained for the controlled variables of the boiler when P_s^* (the steam turbine power set point) was varied in both simulations. Fig. 7 shows the results obtained for the manipulated variables when $P_s{}^*$ was varied. As we expected, the variables return to the set-points for all cases. A slight increase is observed for steam pressure of the superheater when the 20% steam support is considered. The fuel flow as well as air flow decrease when the steam support increase, because less steam from the HRSG is required. On the contrary, water flow from the economizer increases. Fig. 8 shows the results obtained for the controlled variables when P_G^* (the gas turbine power set point) was varied in both simulations. When a step change is applied to the gas turbine power, the variable will return to its set-point because the same local control strategy is considered for both CC and ISCC cases. Fig. 9 shows the results obtained for the manipulated variables in this latter case. The controlled variables return to the set-points for all cases. The fuel flow is reduced when the steam support increased, because less steam produced by HRSG is required.

Figs. 7 and 9 show that the ISCC plant demonstrates lower fuel consumption, w_F. This result holds whether the variation in power demand occurs in the gas turbine or in the steam turbine. The fuel consumption decreases as the steam contribution from the solar plant increases. Figs. 6 and 8 also illustrate that the water level of the drum, L, in the ISCC plant remains constant as the steam supply from SSG varies (for variations of 10% or 20%). The pressure of the steam in the superheater does not change as the extent of solar support increases from 10% to 20%. The gas pressure of the furnace, p_G, and the temperature of the superheated steam, Ts, remain constant as the support from the solar plant increases. The reason why these variables remain nearly constant is the different control loops that operate for each of the variables.

Table 1 shows the percentage fuel savings achieved when using an ISCC plant compared with a CC plant, i.e., the fuel savings realized by introducing the steam from a solar plant. This calculation was performed for solar contributions of 10%, 15% and 20%, which corresponds to possible changes of available solar contribution along the year. It is evident that the amount of fuel saved increases with increasing solar support, as expected. The fact that the simulator can compute these quantities may be very useful for the design and optimal operation of ISCC plants.

Fig. 10 shows the behavior of the heat flow being transferred from the furnace to the superheater (Q_{gs}) when the ISCC plant remains constant as the steam supply from SSG varies (for variations of 10% or 20%) as well as the steam power set-point diminishes at t = 50 s. It appears that the heat support provided by the furnace to the superheater that is required to produce the same power diminishes upon the addition of support provided by the solar plant. When the heat support from the solar plant is bigger, less heat support provided by the furnace to the superheater is required. Therefore, in this case, the furnace uses less fuel to produce the same amount of power. It appears that the heat support provided by the furnace to the superheater that is required to produce the same power diminishes upon the addition of support provided by

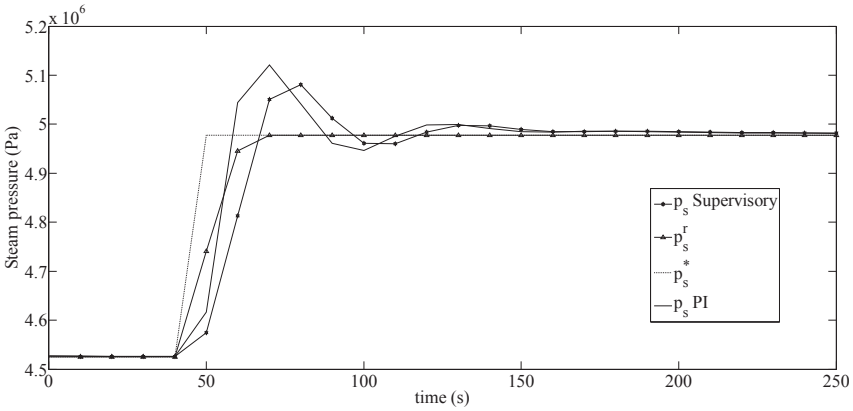

Fig. 5. Steam pressure response with a step-function change in the steam pressure set point at 50 s.

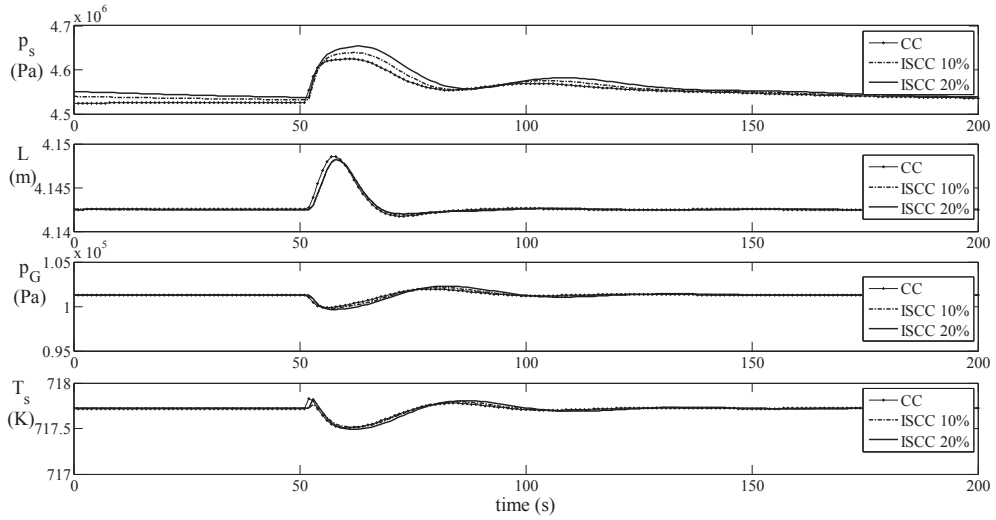

Fig. 6. Boiler response to a step-function change in the steam turbine power set point P_s^* (controlled variables).

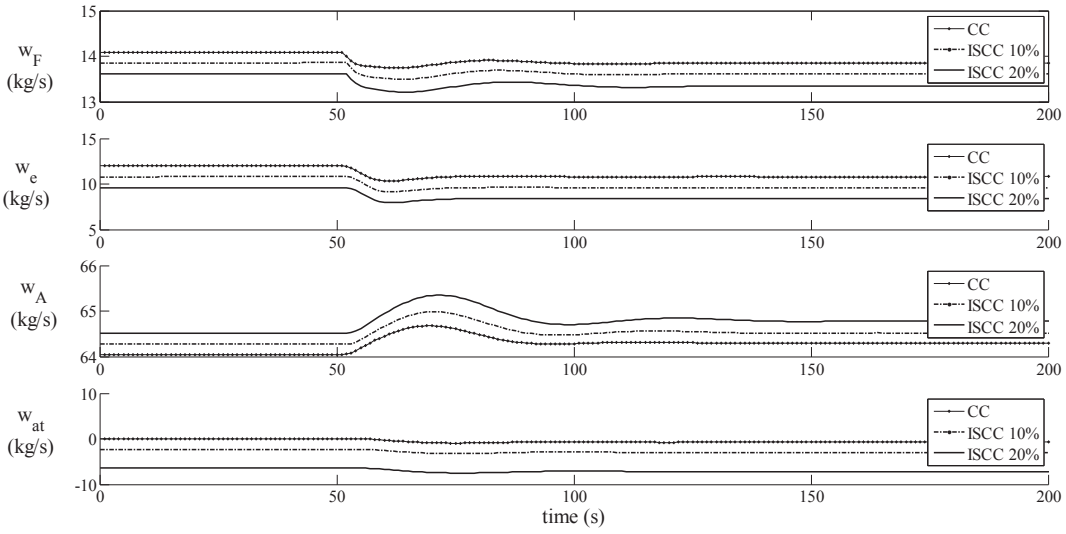

Fig. 7. Boiler response to a step-function change in the steam turbine power set point P_s^*.

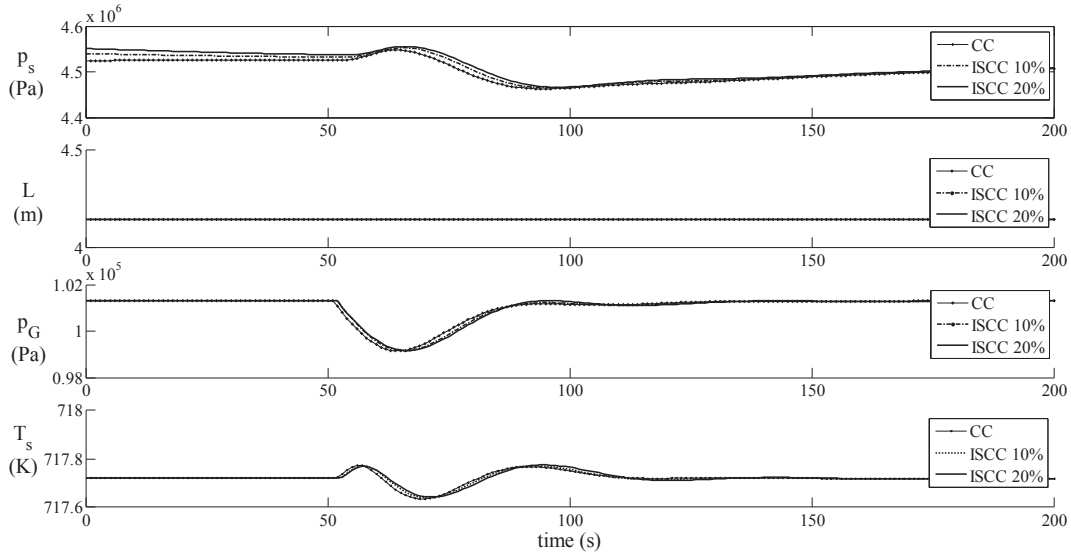

Fig. 8. Boiler response to a step-function change in the gas turbine power set point P_G^*.

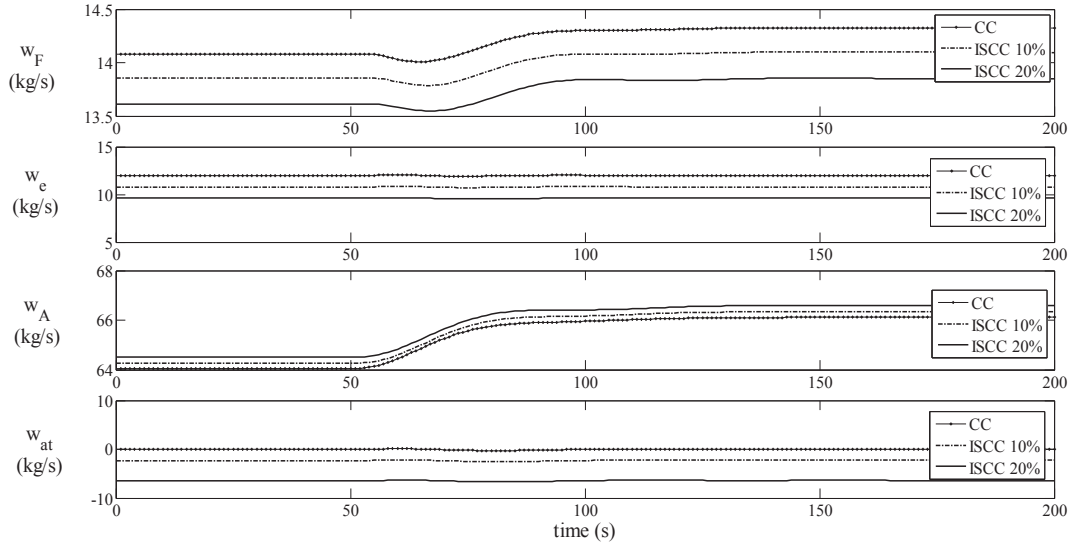

Fig. 9. Boiler response to a step-function change in the gas turbine power set point P_G^*.

the solar plant. When the heat support from the solar plant is bigger, less heat support provided by the furnace to the superheater is required. Therefore, in this case, the furnace uses less fuel to produce the same amount of power.

5.2. Comparison of ISCC plant performance with supervisory MPC and PI control strategies

The fuel consumption savings achieved using supervisory MPC and PI control strategies were calculated. Table 2 compares the simulation-based results obtained using the index given by

Table 1
Savings achieved using an ISCC plant.

	Fuel savings
10% SSG support	1.7%
20% SSG support	3.7%

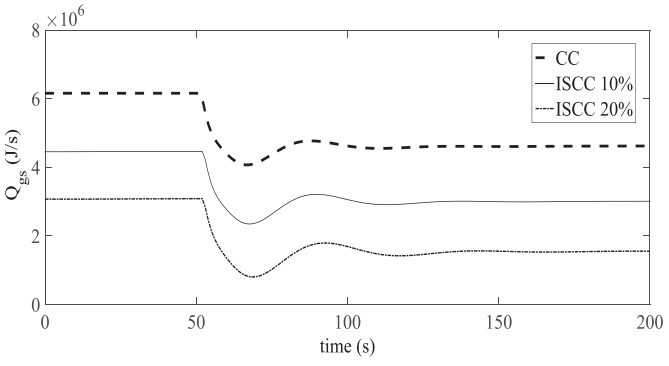

Fig. 10. Heat transferred to the superheater when the steam turbine power set point P_s^* is varied.

Table 2
Evaluation index I_{wF}.

	Supervisory MPC scheme	PI controller	ΔI_{wF}	Savings (%)
I_{wF} kg/s 10%	13.90	13.94	0.04	0.30
I_{wF} kg/s 15%	13.73	13.78	0.05	0.37
I_{wF} kg/s 20%	13.61	13.67	0.06	0.44

equation (32), corresponding to the amount of fuel consumed over a simulation period of 500 s. Considering that an ISCC plant operates over 12 consecutive hours, because the simulator design assumes that the oil is extracted from the storage tank, the savings in fuel consumption amounts to $\Delta w_F = 1754$ kg. Over one year of operation, this savings would be approximately $\Delta w_F = 1{,}280{,}361.6$ kg. In February 2014, the price of natural gas in Chile was 1.44 US$/kg; thus, such a savings would amount to approximately 1,843,721 US$/year. These results demonstrate the relevance of implementing a proper supervisory strategy, particularly when comparing a supervisory MPC strategy with the conventional PI strategy at the regulatory level. For the same power demand, fuel consumption can be better optimized using the MPC-based strategy than with a PI controller alone. It is considered that the plant operates for 24 h because the simulator assumes that the oil is extracted from the storage tank, which allows the oil temperature to remain constant. We assumed that the SSG has a well-sized storage that is used for ensuring the supply of 24-h.

The following is an analysis of the effects of changes in the reference powers for the gas turbine and the steam turbine that allows for a better understanding of how fuel consumption varies in each of these cases. Two types of variations in the reference powers of the steam turbine and the gas turbine were considered. First, the reference power was decreased by 10% and then increased by 10%. This test was performed for both the supervisory MPC strategy and the regulatory-level PI controller. Fig. 11 shows the evolutions of the steam pressure with the supervisory MPC strategy (p_s supervisory), with the PI controller (p_s PI) and with the reference pressure (p_s^r) for a decrease of 10% in the reference power of the steam turbine and in that of the gas turbine. The figure shows that the steam pressure response p_s exhibits a lower overshoot in the case of the supervisory MPC strategy for a decrease in the reference power of the steam turbine. With respect to a change in the reference power of the gas turbine, the difference between the responses of the two controllers is minimal, indicating that both strategies can

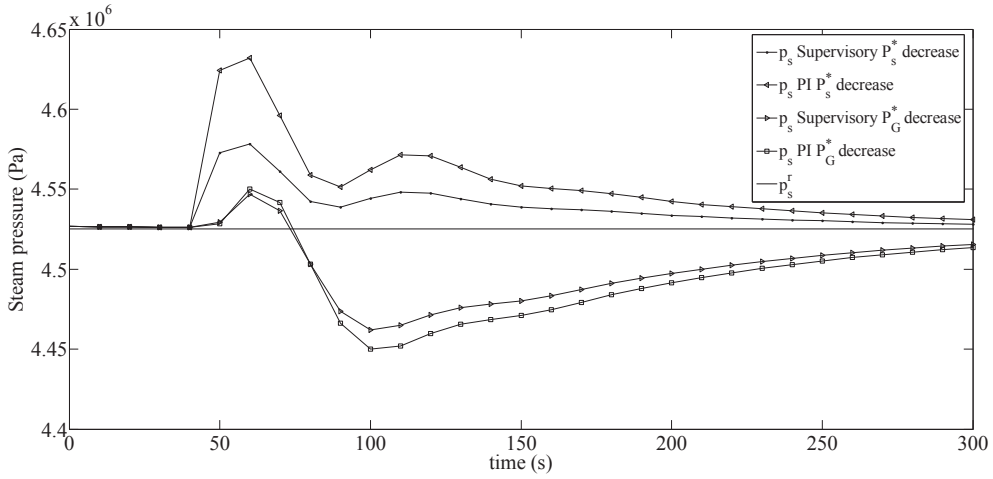

Fig. 11. Steam pressure responses to a step-function change (decrease) in the steam turbine power set point (P_s^*) and in the gas turbine power set point (P_G^*).

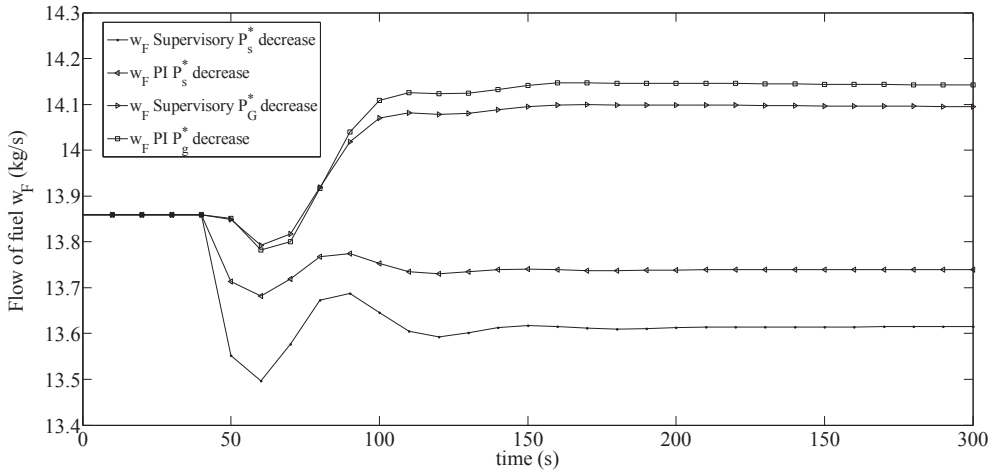

Fig. 12. Fuel flow responses, with PI and supervisory controllers, to a step-function change (decrease) in the steam turbine power set point (P_s^*) and in the gas turbine power set point (P_G^*).

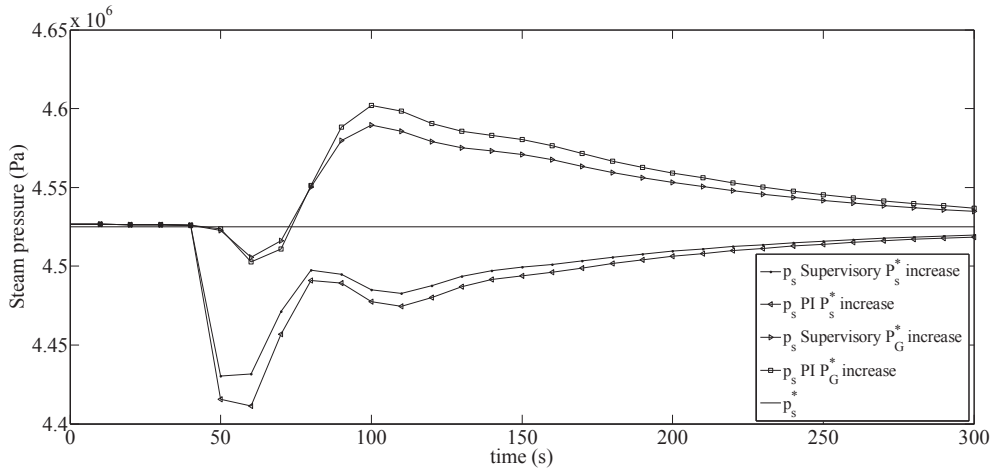

Fig. 13. Steam pressure responses to a step-function change (increase) in the steam turbine power set point (P_s^*) and in the gas turbine power set point (P_G^*).

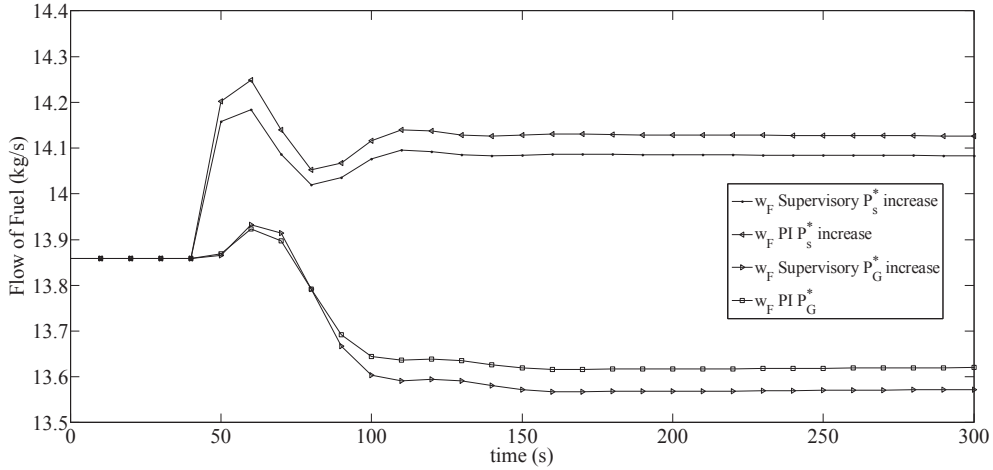

Fig. 14. Fuel flow responses to a step-function change (increase) in the steam turbine power set point (P_s^*) and in the gas turbine power set point (P_G^*).

successfully push the pressure of the steam flow toward its reference value. Fig. 12 shows the evolution of the manipulated variable w_F (fuel flow). It can be observed that when the power demand of the steam turbine (P_s^*) decreases, fuel consumption also decreases. This occurs for both control strategies, but the decrease is greater in the case of a supervisory MPC strategy. That is, under the same operating conditions, less fuel is used when the plant employs a predictive control strategy. When the reference power decreases in the gas turbine, an increase in fuel flow occurs for both strategies, but in the case of the supervisory MPC strategy, the increase in fuel flow is lower.

Fig. 13 shows the evolution of the steam pressure in the superheater when an increase in the reference power of the steam turbine or the gas turbine occurs for both control strategies. As in the previous cases, the results demonstrate that both controllers are able to maintain the steam pressure responses within similar ranges. When the power of the gas turbine increases, less overshoot is observed for the supervisory control strategy. When the power of the steam turbine increases, the steam pressure response is similar for both controllers, but the response with the supervisory MPC strategy is faster. Fig. 14 shows the fuel consumption incurred with the supervisory MPC strategy and the regulatory-level PI controller strategy when the reference powers of the steam turbine and gas turbine are increased. When the power of the steam turbine is increased, an increase in fuel consumption is observed in the auxiliary burner; however, in the case of the system controlled with a supervisory MPC scheme, this increase is much lower. Moreover, when the reference power of the gas turbine increases, the fuel consumption of the afterburner decreases, exhibiting a greater reduction in the case of the supervisory-MPC-controlled system. Thus, the fuel consumption is greater when PI control at the regulatory level is applied.

Table 3
Savings in fuel consumption between the supervisory MPC and PI control strategies.

	I_{wF}(kg/s), Supervisory MPC strategy	I_{wF}(kg/s), PI controller	ΔwF (kg)	Savings (%)
P_s^* (−)	13.61	13.74	0.13	0.92
P_s^* (+)	14.09	14.13	0.04	0.30
P_G^*(−)	14.10	14.14	0.05	0.33
P_G^*(+)	13.66	13.76	0.10	0.73

Table 3 summarizes the savings in fuel consumption achieved by changing the reference values of the steam and gas turbines. The index I_{wF} was calculated using equation (32). Additionally, the differences in fuel consumption between the two control strategies are presented in terms of net values and percentages. In Table 3, a

negative sign (−) represents a decrease in the set point and a positive sign (+) represents an increase in the set point.

6. Conclusions

A dynamic simulator for a combined cycle plant with integrated solar collectors (ISCC plant) was developed. The results obtained from the simulations were compared with the results obtained from simulations of the combined cycle plant alone. Simulations for both cases were performed first with 10% support from a steam flow from the solar plant and then with 20% solar support. In both cases, the results were compared with the values obtained for the combined cycle plant. Among the main results obtained, it was observed that an increase in the steam support from the solar plant diminishes the flow of fuel from the furnace. The flow of heat delivered by the furnace to the superheater diminishes with an increase in the mass flow of steam provided by the solar plant. The supervisory MPC strategy developed for the steam pressure in the superheater allows for the optimization of the fuel flow in the auxiliary burner, thereby allowing the same steam pressure obtained using a PI control strategy to be produced with less fuel consumption for the same power demand. The results demonstrate that in general, fuel consumption is lower under the supervisory MPC strategy. The greatest differences are observed when there is a decrease in the power of the steam turbine and when there is an increase in the power of the gas turbine. The developed simulator is suitable for the study and design of control strategies, for determining the sizing of equipment and for the dynamic optimization of ISCC plants. Further research will focus on multivariable MPC control strategies for ISCC plants and an analysis of the robustness of the MPC controller.

Acknowledgments

This work has been partially supported by the Dirección de Investigación de la Universidad de la Serena project number DIULS DIP 150011, the Solar Energy Research Center SERC-Chile through project CONICYT/FONDAP number 15110019 and the Millennium Institute“Complex Engineering Systems” (ICM: P-05-004-F, CONICYT: FBO16). CVP is grateful for the support provided by CONICYT-Chile through a doctorate scholarship and to the University of La Serena for study leave.

References

[1] Aftzoglou Z. Exploring integration options in the energy sector, including a case study of the integration of solar thermal energy into a combined cycle power plant. MSc Thesis. Delft, The Netherlands: Delft University of Technology; 2011.
[2] Amelio M, Ferraro V, Marinelli V, Summaria A. An evaluation of the performance of an integrated solar combined cycle plant provided with air-linear parabolic collectors. Energy 2014;69:742–8. http://dx.doi.org/10.1016/j.energy.2014.03.068.
[3] Al-Sulaiman F. Exergy analsys of parabolic trough solar collectors integrated with combined steam and organic Rankine cycle. Energy Convers Manag 2014;77:441–9. http://dx.doi.org/10.1016/j.enconman.2013.10.013.
[4] Baghernejad A, Yaghoubi M. Exergy analysis of integrated solar combined cycle system. Renew Energy 2010;35(10):2157–64. http://dx.doi.org/10.1016/j.renene.2010.02.021.
[5] Baghernejad A, Yaghoubi M. Exergo-economic analysis and optimization of integrated solar combined cycle system (ISCCS) using genetic algorithm. Energy Convers Manag 2011;52(5):2193–203. http://dx.doi.org/10.1016/j.enconman.2010.12.019.
[6] Behar O, Kellaf A, Mohamedi K, Belhamel M. Instantaneous performance of the first integrated solar combined cycle system in Argelia. Energy Procedia 2011;6:185–93. http://dx.doi.org/10.1016/j.egypro.2011.05.022.
[7] Behar O, Khellaf A, Mohammedi K, Ait-Kaci S. A review of integrated solar combined cycle systems (ISCCS) with a parabolic through technology. Renew Sustain Energy Rev 2014;39:223–50. http://dx.doi.org/10.1016/j.rser.2014.07.066.
[8] Camacho EF, Berenguel M, Rubio FR. Simulation software package of the Acurex field, E.S.I. Of Sevilla [Internal Report, Sevilla]. 1993.
[9] Camacho E, Berenguel M, Rubio M. Advanced control of solar plants. London: Springer-Verlag; 1997.
[10] Camacho EF, Berenguel Soria M, Rubio FR, Martínez D. Control of solar energy systems. Springer; 2012.
[11] Cau G, Cocco D, Tola V. Performance and cost assessment of integrated solar combined cycle systems (ISCCSs) using CO_2 as heat transfer fluid. Sol Energy 2012;86(10):2975–85. http://dx.doi.org/10.1016/j.solener.2012.07.004.
[12] Dersch J, Geyer M, Herrmann U, Jones S, Kelly B, Kistner R, et al. Trough integration into power plants – a Study-on the performance and economy of integrated solar combined cycle systems. Energy 2004;29(5–6):947–59. http://dx.doi.org/10.1016/S0360-5442(03)00199-3.
[13] Horn M, Füring H, Rheinländer J. Economic analysis of integrated solar combined cycle power plants: a sample case: the economic feasibility of an ISCCS power plant in Egypt. Energy 2004;29(5–6):935–45. http://dx.doi.org/10.1016/S0360-5442(03)00198-1.
[14] Hosseini R, Soltani M, Valizadeh G. Technical and economic assessment of the integrated solar combined cycle power plants in Iran. Renew Energy 2005;30(10):1541–55. http://dx.doi.org/10.1016/j.renene.2004.11.005.
[15] Kelly B, Herrmann U, Hale MJ. Optimization studies for integrated solar combined cycle systems. In: Proceeding of Solar Forum 2001, Solar Energy The Power to Choose, Washington DC, USA, April 21–25 2001, vol. 1. New York: ASME; 2001. p. 1–7.
[16] Lambert T, Hoadley A, Hooper B. Process integration of solar thermal energy with natural gas combined cycle carbon capture. Energy 2014;74:248–53. http://dx.doi.org/10.1016/j.energy.2014.06.038.
[17] Nezammahalleh H, Farhadi F, Tanhaemami M. Conceptual design and techno-economic assessment of integrated solar combined cycle system with DSG technology. Sol Energy 2010;84(9):1696–705. http://dx.doi.org/10.1016/j.solener.2010.05.007.
[18] Ordys A, Pike A, Johnson M, Katebi R. Modelling and simulation of power generation plants. London: Springer-Verlag; 1994.
[19] Price H, Lüpfert E, Kearny D, Zarza E, Cohen G, Gee R, et al. Advances in parabolic trough solar power technology. J Sol Energy Eng 2002;124(2):109–25. http://dx.doi.org/10.1115/1.1467922.
[20] Reid R, Prausnitz J, Poling B. Properties of gases and liquids. Nueva York: McGraw-Hill Co; 1987.
[21] Reynolds W. Thermodynamic properties in SI, USA. Mechanical Eng. Dept. Stanford University; 1979.
[22] Sáez D, Cipriano A, Ordys A. Optimization of industrial processes at supervisory level. Application to control of thermal power plants. London: Springer-Verlag; 2002.
[23] Spelling J, Favrat D, Martin A, Augsburger G. Thermoeconomic optimization of a combined-cycle solar tower power plant. Energy 2012;41(1):113–20. http://dx.doi.org/10.1016/j.energy.2011.03.073.